Tolerance Analysis and Desensitization to Parallelism in Afocal Systems of Fabry-Perot Spectrometers

Lu Zhang, Bo Li, Xiaoxu Wang, Hanshuang Li, and Guochao Gu

Abstract— **Existing research on Fabry-Perot (FP) spectrometers lacks tolerance analysis and desensitization for the parallelism of afocal systems, leading to scenarios where, despite afocal systems being satisfactory in design, their parallelism deteriorated during actual production. Therefore, this letter proposes a tolerance analysis and desensitization optimization method for the parallelism of afocal systems applied to FP spectrometers. By creating multiple zooms, we can intuitively analyze the impact of each tolerance on parallelism, and perform desensitization optimization of parallelism based on the characteristic angle changes dictated by the FP etalon. Utilizing this method, we conduct a tolerance analysis and desensitization optimization of parallelism for afocal systems, achieving a parallelism-insensitive afocal system and verifying the effectiveness of the method.**

Index Terms— **Fabry-Perot, spectrometers, desensitization, tolerance.**

I. INTRODUCTION

SPECTROMETER is an important measurement tool [1]. Fabry-Perot (FP) spectrometer is a kind of spectrometer with the advantages of miniaturization, high luminous flux, and high spectral resolution, which can be applied to ozone and greenhouse gas observation [2], [3], [4].

Various studies and analyses have been conducted on FP spectrometers. Dylan et al. designed an FP spectrometer for greenhouse gas observation, describing the spectrometer design and performing spectral inversion analysis [5], [6]; Lingjun Gu et al. analyzed the relationship between the signal-to-noise ratio and the parameters of the FP spectrometer, and design an FP spectrometer that meets specific signal-to-noise ratio requirements [7]; G. A. Gary et al. developed a 3FP cascade spectrometer for UV observation, analyzing the materials, surface roughness, and other parameters of FP etalons from a manufacturing perspective [8]; R Rami Mannila et al.

designed an FP spectrometer that can be accommodated within a 3U volume, analyzing and presenting the system parameters and FP structural design [9], [10].

The existing designs and research on FP spectrometers predominantly focus on analyzing and optimizing the parameters of the FP etalon. However, there is a lack of research on the analysis and optimization concerning the impact that the coupling between the FP devices and other components, such as telescope systems or afocal systems, has on performance. If the parallelism of the light beam emitted by an afocal system is poor, light beams entering the same field of view (FOV) will have multiple exit angles upon emission. After interfering through the FP etalon, these beams emit light at different intensities (angles). When converged by the imaging system, part of the light from the same FOV falls onto adjacent pixels, adversely affecting the actual spectral resolution or the peak wavelength corresponding to each pixel.

Therefore, this study investigates how parallelism in afocal systems is affected under tolerance perturbation. We proposed a tolerance analysis and desensitization optimization method for the afocal system of the FP spectrometer. To observe the impact of various tolerances clearly and straightforwardly on the system's parallelism, zooms are applied to each tolerance of every surface. According to the characteristics of the FP etalon, different constraints for the parallelism of each FOV are established, optimizing the system through desensitization. This led to the realization of an afocal system design with excellent parallelism under reasonable tolerances. The results demonstrate that our approach is suitable for the tolerance analysis and desensitization optimization of FP afocal systems.

II. THEORETICAL ANALYSIS

The impact of parallelism on spectral resolution or the corresponding peak wavelength is a complex process. It involves analyzing the proportion of light rays at other angles to those at the intended angle, obtaining the actual light intensity values to deduce the full width at half maximum (FWHM) and the corresponding wavelength. However, the aim of our study is to propose a tolerance analysis and a desensitization method for parallelism, making the afocal system a manufacturable reality. Therefore, we demonstrate using the simple case of peak wavelength. We require that, for a given FOV in the afocal system, all rays within the emitted beam, after tolerance-induced perturbations, must remain within the desired angular range. This method provides a stricter and more calculation-friendly alternative to proportion-based ray analysis.
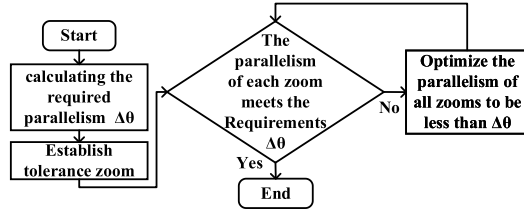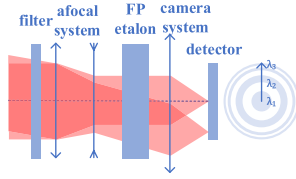
Fig. 1. Optimization workflow.

Fig. 2. Schematic diagram of the FP spectrometer.

For the FP etalon, the relationship between the peak wavelength λ and the incidence angle θ can be expressed as:

$$m\lambda = 2nhcos\theta \qquad (1)$$

where m is the order of interference, h is the thickness of the etalon. When the peak wavelength changes by $\Delta\lambda$ the equation can be represented as:

$$m\left(\lambda + \Delta\lambda\right) = 2nhcos(\theta + \Delta\theta) \qquad (2)$$

where $\Delta\theta$ is the change in angle. Thus, for a change $\Delta\lambda$, $\Delta\theta$ can be calculated as:

$$\Delta\theta = \arccos\left(\frac{m\left(\lambda + \Delta\lambda\right)}{2nh}\right) - \theta \qquad (3)$$

Parallelism is set as the difference between the peripheral rays (upper and lower rays) and the principal ray:

$$\theta_{R2} = \theta_{up} - \theta_p, \theta_{R3} = \theta_{down} - \theta_p \qquad (4)$$

Where θ_{up} is the angle of the upper ray, θ_p is the angle of the principal ray, and θ_{down} is the angle of the lower ray.

The design process involves initially calculating the parallelism requirement $\Delta\theta$ for each FOV. Subsequently, for each surface, we construct zooms accounting for all tolerances and assess the parallelism for these zooms. If they do not meet the requirement of $\Delta\theta$, we optimize and control the parallelism of all zooms to ensure it falls below the $\Delta\theta$ of the corresponding FOV. After optimization, the parallelism for each FOV is reassessed to verify compliance with the $\Delta\theta$ requirement, concluding the optimization process upon satisfaction. The optimization workflow is illustrated in Fig. 1.

III. SIMULATION ANALYSIS

The schematic diagram of the FP spectrometer is shown in Fig. 2, which consists of a filter, an afocal system, an FP etalon, and an imaging system. The filter eliminates unwanted spectral bands, the afocal system magnifies the beam in the FOV, adjusts the angle to enlarge and reduces the beam aperture to adapt to the FP etalon, and the etalon performs equi-inclination interference on the beam, where different incident angles correspond to different peak wavelengths.

According to the interference characteristics of the FP etalon, different angles correspond to different wavelengths,

TABLE I
MAIN PARAMETERS OF THE AFOCAL SYSTEM AND FP ETALON

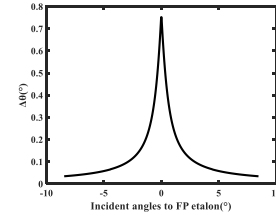| parameters	numerical value
FOV (°)	13°
Magnification	1.3
Air gap refractive index	1
Air gap length (mm)	0.105
Wavelength range (nm)	1635~1675
Wavefront differential tolerance performance	>80%(@0.5λ, λ=1655nm)

Fig. 3. The angular changes corresponding to the incident angle when the wavelengths vary by 0.15 nm.

TABLE II
FOV AND CORRESPONDING BEAM PARALLELISM LIMITS

FOV (°)	5.0992	5.8070	6.1600	6.5120
Beam parallelism restriction (°)	0.0442	0.0389	0.0366	0.0347

which, through the imaging system's convergence, translate into different wavelengths corresponding to different radii centered around the detector's origin. Therefore, by scanning across the field from the edge to the center, it traverses all wavelengths, thereby completing the sampling of all wavelengths.

The main parameters regarding the afocal system and FP etalons are shown in Table I.

The free spectral range of the etalon was 13 nm, and at each incident angle, the etalon corresponded to three peak wavelengths. By utilizing the properties of the arccosine function, we understood that changes in the longer wavelength set resulted in smaller $\Delta\theta$ changes. We calculated the incident angles for a series of longer peak wavelengths to the FP etalon, and assessed the variations in these angles as the wavelengths change by 0.15 nm(required value), these relationships are depicted in Fig. 3.

According to Figure 3, the center FOV has a more relaxed restriction on parallelism, while the edge FOV has a more stringent restriction. We used this as a basis for limiting the parallelism of the beam exiting the afocal system. Since the system is rotationally symmetric, the forward FOV is identical to the negative FOV, and we set up four sampling points on the FOV. The corresponding FOV and beam parallelism constraints are presented in Table II.

Based on the parameters in Table I, we designed an afocal system starting from the initial structure of a Galilean telescope system, which resulted in an afocal system comprising three spherical lenses.

The parallelism of four sampling points in the afocal system was evaluated and summarized in Table III. The table shows that before introducing tolerance perturbations, the parallelism across each FOV satisfactorily met the requirements.

The afocal system, comprising three lenses with six surfaces, has its surfaces ordered according to the direction of
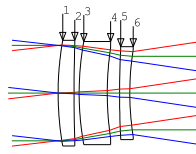
Fig. 4. Optical path diagram of afocal system, the numbers represent the surface numbers.

TABLE III
PARALLELISM OF EACH FOV BEFORE TOLERANCE PERTURBATION

FOV (°)	5.0992	5.8070	6.1600	6.5120
θ_{R2} (°)	0.0020	0.0027	0.0027	0.0027
θ_{R3} (°)	0.0007	0.0040	0.0046	0.0051
Beam parallelism requirement (°)	0.0442	0.0389	0.0366	0.0347

TABLE IV
DISTRIBUTION OF TOLERANCES

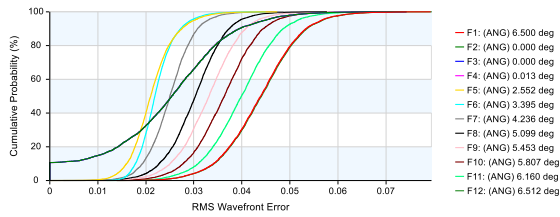| Surface	R/mm	L/mm	D/mm	T/rad
1	0.02	0.07	0.020	0.0005
2	0.20	0.04	0.030	0.0005
3	0.01	0.03	0.009	0.0003
4	0.01	0.03	0.010	0.0003
5	0.04	0.07	0.060	0.0005
6	0.05	0.05	0.025	0.0005

Fig. 5. Wavefront differential tolerance analysis before optimization.

light propagation. We defined surface radius tolerances as R, thickness tolerances as L, eccentricity tolerances as D, and tilt tolerances as T. Using optical design software, we analyzed how variations in surface radius ($\pm$R), thickness ($\pm$L), eccentricity ($\pm$D), and tilt ($\pm$T) impact the wavefront error and the corresponding probabilities in the afocal system, as measured by the RMS (root mean square). By properly allocating and adjusting the values of these tolerances (Table IV), the system meets the requirement of achieving an RMS wavefront error of less than 0.5 wavelengths with an 80% probability in the as-built condition (Fig. 5).

While the wavefront differential tolerance analysis at this stage can help us determine a reasonable allocation of tolerances and analyze the quality of the wavefront, it does not enable us to analyze the impact of tolerance perturbations on parallelism. Therefore, we cannot be certain that parallelism can meet the requirements in Table III during actual manufacturing.

To analyze the impact of tolerance perturbations more intuitively on parallelism, we have set eight zooms for each surface. Each zoom alters only one parameter, including deviations of $\pm$R from the original radius, $\pm$L for original thickness, $\pm$D for eccentricity, and $\pm$T for tilt, thus simulating the deviation of surface parameters from their ideal state during actual manufacturing. In total, 49 zooms have been set (six surfaces and one original zoom). We summarized the parallelism data for each zoom state in Fig. 6, allowing
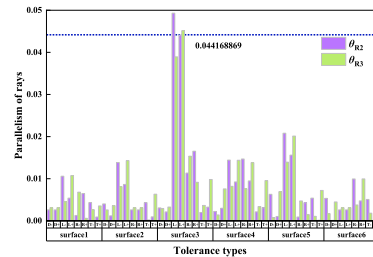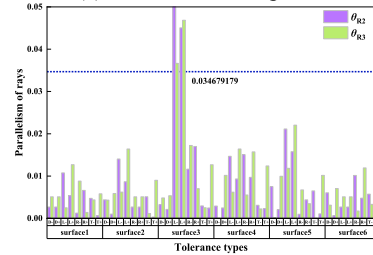

(a) FOV of 5.0992 degrees
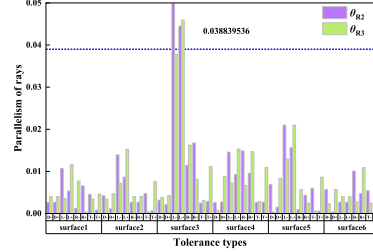
(b) FOV of 5.8070 degrees
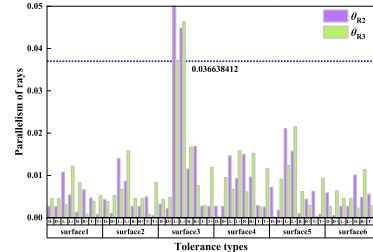
(c) FOV of 6.160 degrees

(d) FOV of 6.512 degrees

Fig. 6. Parallelism corresponding to each tolerance after perturbation.

us to understand the parallelism status under corresponding tolerance conditions.

Based on the information from Table III and Fig. 5 and Fig. 6, we can determine that even when the parallelism of the afocal system is good during the design phase, and the wavefront differential tolerance performance is also favorable, the parallelism of the beam under corresponding tolerance conditions may not necessarily be satisfactory. Additionally, the beam incident on the etalon from the same FOV will exhibit some angular difference between the peripheral rays and the principal ray upon exiting, potentially leading to changes in the peak wavelength or the FWHM.

To enhance the parallelism of the outgoing beams of the afocal system under given tolerances, making it feasible for actual use, we optimized to reduce sensitivity to beam parallelism deviations. We restricted the parallelism for all zooms to prompt the software to optimize a suitable system, adhering to the parallelism criteria specified in Table II. This ensures that the parallelism of all zooms meets the requirements.

(a) FOV of 5.0992 degrees

(b) FOV of 5.8070 degrees

(c) FOV of 6.160 degrees
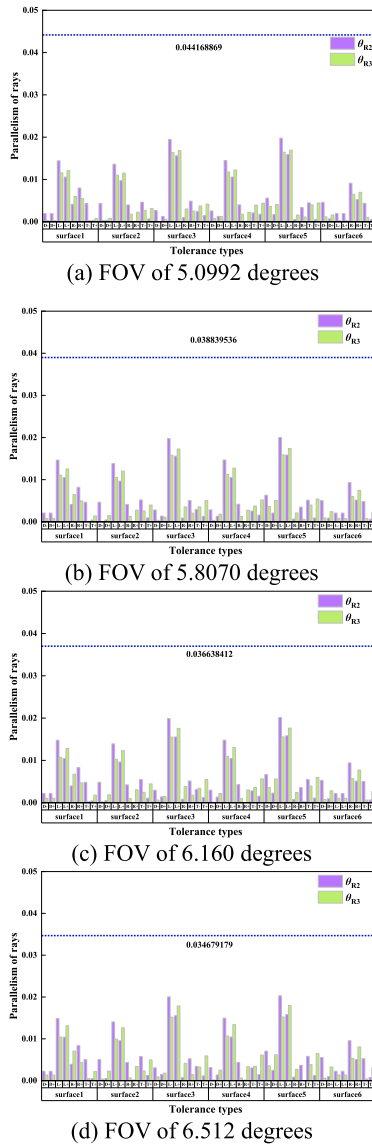

(d) FOV of 6.512 degrees

Fig. 7. Parallelism analysis for different zooms after desensitization optimization.
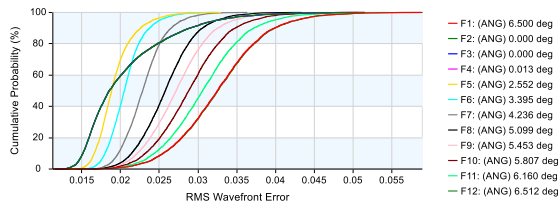

Fig. 8. Wavefront differential tolerance analysis after desensitization optimization.

Essentially, the optimized system will guarantee that the parallelism satisfies the requirements under all the tolerance perturbations we have set.

Following the optimization, we reassessed the parallelism at every zoom and compiled the findings in Fig.7. The wavefront differential tolerance performance post-optimization is depicted in Fig.8.

Fig. 7 and Fig. 8 demonstrate that, by applying the beam parallelism desensitization optimization method for the afocal system introduced in this study, the wavefront differential

tolerance performance remains in a favorable state. The beam parallelism for each FOV meets the requirements calculated in Table II under every tolerance condition. Compared to the value before optimization, there has been an average improvement of approximately 30%. This indicates the effectiveness of the method proposed in this study.

IV. CONCLUSION

The design process of conventional FP spectrometers does not analyze and optimize the parallelism of the beams in each FOV under tolerance conditions. However, the beam's parallelism affects the FP spectrometer's exit wavelength position and FWHM. Hence, this study introduces a tolerance analysis and desensitization optimization method for the parallelism of an afocal system. By adding zooms for each tolerance, the parallelism data under each tolerance can be directly observed, and the parallelism for each zoom is restricted and optimized according to the angular variation characteristics of the FP etalon. The optimization results in an afocal system that meets the parallelism requirements and achieves a favorable wavefront differential tolerance performance under the corresponding tolerance conditions, with an average parallelism improvement of about 30%. This validates the effectiveness of the method proposed in this study, offering insights for the design and production of FP spectrometers suitable for practical applications, and applicable to the design and manufacturing of FP spectrometers.

REFERENCES

[1] G. Thuillier, P. Zhu, M. Snow, P. Zhang, and X. Ye, "Characteristics of solar-irradiance spectra from measurements, modeling, and theoretical approach," *Light, Sci. Appl.*, vol. 11, no. 1, p. 79, Mar. 2022, doi: 10.1038/s41377-022-00750-7.

[2] M. Pisani and M. E. Zucco, "Compact imaging spectrometer combining Fourier transform spectroscopy with a Fabry–Perot interferometer," *Opt. Exp.*, vol. 17, no. 10, p. 8319, May 2009, doi: 10.1364/oe.17.008319.

[3] T. Nagayama et al., "A high-spectral resolution tandem Fabry–Perot spectrometer for 17-micrometer wavelength," *Proc. SPIE*, vol. 6269, Jun. 2006, Art. no. 626948, doi: 10.1117/12.671463.

[4] J. Nikoleyczik, A. Kutyrev, H. Moseley, and S. Veilleux, "Wide field of view spectroscopy using solid Fabry–Perot interferometers," *Proc. SPIE*, vol. 9908, Aug. 2016, Art. no. 99085N, doi: 10.1117/12.2232864.

[5] D. Jervis et al., "The GHGSat-D imaging spectrometer," *Atmos. Meas. Techn.*, vol. 14, no. 3, pp. 2127–2140, Mar. 2021, doi: 10.5194/amt-14-2127-2021.

[6] M. Ligori, L. Bradbury, R. Spina, R. E. Zee, and S. Germain, "GHGSat constellation: The future of monitoring greenhouse gas emissions," Space Flight Lab., Univ. Toronto Inst. Aerosp. Stud., Toronto, ON, Canada, GHGSat Inc., Montreal, QC, Canada, Tech. Rep. SSC19-V-02, 2019.

[7] L. Gu, Q. Pan, X. Chen, and W. Shen, "Design and analysis of optic system for satellite-borne miniature high-resolution greenhouse gas monitoring instrument," *Proc. SPIE*, vol. 12617, pp. 2045–2051, Apr. 2023, doi: 10.1117/12.2666883.

[8] G. A. Gary, E. A. West, D. Rees, J. A. McKay, M. Zukic, and P. Herman, "Solar CIV vacuum-ultraviolet Fabry–Perot interferometers," *Astron. Astrophys.*, vol. 461, no. 2, pp. 707–722, Jan. 2007, doi: 10.1051/0004-6361:20066035.

[9] R. Mannila, A. Näsilä, K. Viherkanto, C. Holmlund, I. Nakki, and H. Saari, "Spectral imager based on Fabry–Perot interferometer for Aalto-1 nanosatellite," *Proc. SPIE*, vol. 8870, Sep. 2013, Art. no. 887002, doi: 10.1117/12.2023299.

[10] R. Mannila, A. Näsilä, J. Praks, H. Saari, and J. Antila, "Miniaturized spectral imager for Aalto-1 nanosatellite," *Proc. SPIE*, vol. 8176, Oct. 2011, Art. no. 817628, doi: 10.1117/12.897999.